High Order Time Shift Keying Modulation for Ambient Backscatter Communications

Jixiang Chen, Quansheng Guan, *Senior Member, IEEE*, Yue Rong, *Senior Member, IEEE*, Dong Li, *Senior Member, IEEE*, Weiqi Chen, Hua Yu, *Member, IEEE*

***Abstract*—Ambient backscatter communication (AmBC) is a newly cutting-edge technology for the Internet of Things, which utilizes the ambient radio frequency signal as the carrier to transmit information. Existing works focus on the simple on-off keying modulation which has low channel utilization. However, it is not desirable to develop the high-order modulation in the power domain due to the weak strength of the backscattered signal. In this paper, we extend the high-order modulation in the time domain instead, i.e., high-order time shift keying (TSK). Since the channel coherent time is unknown at the receiver and the tag, the detection methods with training symbols will have a huge performance degradation if the channels are changed and training symbols become outdated. To overcome this challenge, we further propose the transition-aided TSK (TA-TSK) modulation and the frequency-shifting TSK (FS-TSK) modulation, which do not need to send training symbols at the tag. These two methods can work well even if the channel coherent time is as short as one time slot. Meanwhile, the detection methods for TSK are developed and the corresponding closed-form bit-error-rate (BER) expressions are obtained. Simulation results show that a high modulation order is more suitable for the M-ary phase shift keying source than the complex Gaussian source. The high order TSK can provide at least 2 dB signal-to-noise ratio (SNR) gain at the same BER compared to the on-off keying.**

***Index Terms*—Ambient backscatter, time shift keying, modulation, detection, bit-error-rate.**

I. Introduction

Due to its low power consumption and low cost, ambient backscatter communication (AmBC) has been considered as an appealing technology for the Internet of things (IoT) [2]–[5] . In AmBC, there is no dedicated radio frequency (RF) source for tag backscattering compared to conventional monostatic or bistatic backscatter communication [6]–[9]. Instead, ambient signals like TV signals [10], FM signals [11], [12] and Wi-Fi signals [13]–[17] etc., can be used as source signals for realization of AmBC.

In AmBC, the strength of the backscattered signal is weak due to its low reflection efficiency and a large path loss [18]–[21]. Considering also the low-cost and low-complexity tag, most of the works on the AmBC system adopt binary modulation schemes, e.g., on-off keying (OOK) [10] [13], [22]–[32], which means a low channel utilization for AmBC. The OOK modulation belongs to the binary amplitude shift keying (ASK). If we increase the modulation order in the power domain, the difference in strengths of the backscattered signals will be small under the weak backscattered signal, which leads to poor detection performance. Thus, the high-order modulation in the power domain is not practical for the tag. For this reason, the high-order modulation in AmBC should be explored in other signal domains.

Existing works have explored high-order modulation for AmBC. The authors investigate the high order time shift keying to increase the channel utilization [1]. Both coherent and non-coherent transmission schemes are studied. For the space domain [33], the authors employ multiple antennas at the tag and the reader to realize the space shift keying increasing the communication rate. The authors in [35] explores the multiple frequency shift keying modulation in which the direct link interference are removed by multiple frequency bands and passband filters at the receiver. In [36], the authors propose the high order phase-shift keying for AmBC and derive the optimal energy detector under the source with a complex Gaussian distribution. For the sake of understanding, we make a comparison between the high order modulations over different signal domains in Table I.

There have been already high order modulation schemes proposed for orthogonal frequency division multiplexing (OFDM) ambient sources based AmBC. The authors in [37] propose two modulation schemes including phase-shift keying and delay-shift keying in ambient OFDM pilot-aided backscatter communications. The authors in [38] realize high order modulation by shifting energy to null subcarriers with OFDM source signals. The author in [39] investigates the noncoherent maximum likelihood (ML) detection problem for a general Q-ary signal constellation over the ambient OFDM source. Note that these methods are designed exclusively for the OFDM ambient source and not applicable to other sources.

This paper proposes the basic time shift keying (TSK) modulation and further proposes other two TSK based mod-

This work was supported by the National Natural Science Foundation of China under Grants U23A20281, 62341129 and 62192712, and the Science and Technology Planning Project of Guangdong Province of China under Grant 2023A0505050097. This work was supported in part by the Science and Technology Development Fund, Macau, SAR, under Grant 0188/2023/RIA3. This paper was presented in part [1] at the 2023 IEEE/CIC International Conference on Communications in China (ICCC Workshops), Dalian, China, 2023.

Jixiang Chen, Quansheng Guan, and Hua Yu are with the School of Electronic and Information Engineering, South China University of Technology, Guangzhou 510640, China (Corresponding author: Quansheng Guan; e-mail: eejxchen@mail.scut.edu.cn; eeqshguan@scut.edu.cn; yuhua@scut.edu.cn).

Yue Rong is with the School of Electrical Engineering, Computing and Mathematical Sciences, Curtin University, Bentley, WA 6102, Australia (e-mail: y.rong@curtin.edu.au).

Dong Li is with the School of Computer Science and Engineering, Macau University of Science and Technology, Macau 999078, China (e-mail: dli@must.edu.mo).

Weiqi Chen is with School of Internet Finance and Information Engineering, Guangdong University of Finance, Guangzhou, China (e-mail: 47-119@gduf.edu.cn).

TABLE I
ADVANTAGES AND LIMITATIONS OF HIGH ORDER MODULATIONS IN DIFFERENT SIGNAL DOMAINS.

Signal domains	Advantages	Limitations
Time	Reducing the interference to the legacy users; No additional hardware or frequency bands; Less or no training symbols and no detection threshold	Suffering from the direct link interference
Frequency	Removing the direct link interference, and increasing the communication rate; No training symbols and no detection threshold	Requiring frequency shift at the tag and multiple frequency bands and filters at the receiver
Space	Removing the direct link interference, and increasing the communication rate	Requiring additional hardware at the tag and the reader
Power	Increasing the communication rate	Requiring multiple impedance; Requiring more training symbols to estimate parameters; Multiple detection thresholds for each source; Suffering from the direct link interference
Phase	Increasing the communication rate	Requiring multiple impedance; Requiring more training symbols to estimate parameters; Multiple detection thresholds for each source; Suffering from the direct link interference

ulations to handle unknown channel changes. The basic TSK modulation has been proposed in [1], which is included in this paper. Besides, this paper investigates additional theoretical analysis and simulations for the other two TSK based modulations. To be specific, this paper proposes to implement high-order TSK for AmBC, which extends the modulation order in the time domain to increase the channel utilization. TSK backscatters the ambient signals in one time slot and this time slot is referred to as the active time slot. TSK modulates its information at the position index of the active time slot. In this sense, the channel utilization can be increased compared to the binary modulation schemes.

To demodulate the TSK signal, it is critical to determine the position of the active time slot in which the tag backscatters ambient source signals. Due to the complex form of signals, it is not guaranteed that the power of the superposition of the source and the backscattered signals in the active slot is larger than that of the signals in the inactive slots. Therefore, the complex signals bring uncertainty in detecting the active time slot. This uncertainty can be readily addressed by using training symbols, although the training symbols introduce extra overhead for AmBC. We also find that the superimposed signal in the active time slot may be the maximum value or the minimum value among all time slots. Then, the inactive slots can be regarded as potential training symbols. Our finding will give rise to a new signal detector without any training symbols for high-order TSK.

Moreover, considering the channel coherent time is unknown at the receiver and the tag. When the channel is changed, the parameters estimated by the training sequence may be outdated, and the corresponding detection will have a huge performance degradation. To overcome this challenge, we propose two TSK based schemes without the training symbols including the transition-aided TSK (TA-TSK) modulation and the frequency-shifting TSK (FS-TSK) modulation. In TA-TSK, the tag only backscatters signals during the half of the active time slot. In this sense, there is an energy transition in a slot. The detection of TA-TSK relies on the relative energy difference between the first half and the second half in one time slot so that the detection will not be affected by channel changes during transmissions. Using FS-TSK, the backscatter signals are shifted outside the frequency band of the source. The signals in inactive time slots contain only noise but not source signals, while signals in active time slots include both backscattered signals and noise. Thus, the changes of channels also do not affect the detection of FS-TSK.

The main contributions are summarized as follows.

- We propose the basic TSK modulation for AmBC to implement high order modulation in the time domain. Three detection approaches are proposed for our proposed basic TSK techniques, including maximum likelihood detector with training symbols (ML-TS), energy detector with training symbols (ED-TS) and energy detector without training symbols (ED-NoTS). Their closed-form bit-error-rates (BERs) are derived for both complex Gaussian (CG) sources and M-ary phase shift keying (M-PSK) sources. We find that ML-TS is equivalent to ED-TS under the CG source.
- We propose TA-TSK and FS-TSK for AmBC to further handle the unknown channel coherent time for AmBC. For TA-TSK, we propose a detection method based on energy detection and the theoretical BER under both CG sources and M-PSK sources are obtained. For FS-TSK, energy detection with the help of one pass-band filter is proposed and its theoretical BER is obtained.
- Simulation results are provided to verify the performance

of the proposed three modulation methods and verify our theoretical analysis. In the same BER level, at least 2 *dB* signal-to-noise ratio (SNR) gain is achieved for the the high order TSK compared to the on-off keying in terms of the PSK sources.

The remainder of this paper is organized as follows. Section II describes the TSK model and signal model for AmBC. In Section III, the detection methods for TSK, TA-TSK and FS-TSK are developed. Simulation results are provided in Section IV. Finally, Section V concludes this paper.

Notations: Scalars are denoted by lowercase letters, while vectors and matrices are represented by bold letters. $\mathbf{0}_{\mathrm{m\times n}}$ and $\mathbf{1}_{\mathrm{m\times n}}$ represent $m \times n$ zero and all-ones matrices respectively. $\mathbf{I}_N$ denotes the identity matrix of size N. We use $|x|$ to denote the absolute value of number x. We use $||\mathbf{x}||$ to denote the Frobenius norm. $\mathcal{N}(\mu, \sigma^2)$ and $\mathcal{CN}(\mu, \sigma^2)$ denote the real Gaussian and complex Gaussian distribution with mean μ and variance σ^2, respectively, and χ_v^2 denotes the central chi-squared distribution with v degrees-of-freedom (DoF). The function $erfc(x) = \frac{2}{\sqrt{\pi}} \int_x^{+\infty} e^{-t^2} dt$ returns the complementary error function evaluated at x. The function $\Gamma(\cdot)$ denotes the gamma function.

II. High-order TSK for AmBC

A. Model for High-order TSK

Assume that there are L time slots for a TSK symbol and only one time slot is activated to backscatter signals. Thus, the tag can transmit $\log_2 L$ bits during one TSK symbol. The number L usually takes an integer power of 2, so that a one-to-one mapping between input bits and active time slot indices can be realized. A case of $L = 4$ is shown in Table II, where an active slot sets two bits.

TABLE II
Mapping between the input bits and time slot index

Input bits	Active time slot index
{0, 0}	1
{0, 1}	2
{1, 0}	3
{1, 1}	4

B. Signal Model for AmBC

An AmBC system often consists of an ambient source, a tag and a reader. Each of them is assumed to be equipped with a single antenna. We denote the channel from the source to the reader as a direct channel h_d, the channel from the source to the tag as a forward channel h_f, and the channel from the tag to the reader as a backward channel h_b, respectively.

The backscattered signals are weak and we prolong the duration of the TSK symbol to reduce detection errors. We assume that there are N backscattered signals in one time slot. That is, one TSK symbol includes LN signals. Let the n-th backscattered symbol in the l-th time slot as $x_l(n) \in \{0, 1\}$, and the source symbol as $s_l(n)$. Then the n-th received signal of the l-th time slot at the reader is

$$y_l(n) = h_d s_l(n) + h_b h_f \alpha x_l(n) s_l(n) + w_l(n), \tag{1}$$

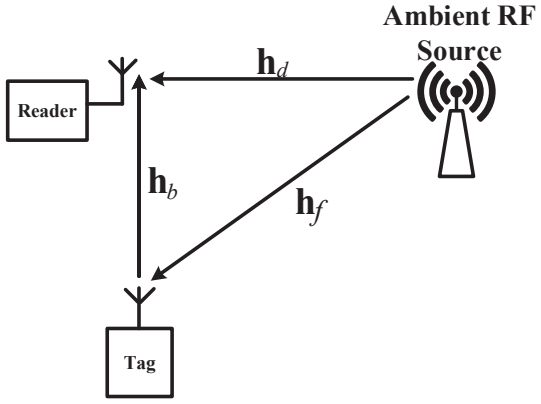

Fig. 1. System model of ambient backscatter communications.

where $n = 1, 2, \cdots N, l = 1, 2, \cdots L$, α is a coefficient representing the scattering efficiency and antenna gain, and $w_l(n)$ is the zero-mean additive white Gaussian noise (AWGN) with variance σ_w^2. Let $h_0 = h_d$ and $h_1 = h_d + h_b h_f \alpha$ for notation simplicity, and then we get

$$y_l(n) = \begin{cases} h_0 s_l(n) + w_l(n), x_l(n) = 0, \\ h_1 s_l(n) + w_l(n), x_l(n) = 1. \end{cases} \tag{2}$$

The tag can adopt one of the basic TSK, TA-TSK and FS-TSK modulations to convey its information, and only one time slot is activated by different ways to reflect ambient signal.

*1) **Basic TSK**:* In the active time slot, the tag backscatters ambient signals while absorbing signals in the other time slots. In L time slots, the backscattered symbols vector of the tag by the basic TSK modulation is

$$\mathbf{X} = [\mathbf{x}_1, \mathbf{x}_2, \cdots, \mathbf{x}_L], \tag{3}$$

where $\mathbf{x}_l, l = 1, 2, \cdots, L$, is the backscattered symbols vector in one time slot, and $\mathbf{x}_l \in \{\mathbf{0}_{1\times \mathrm{N}}, \mathbf{1}_{1\times \mathrm{N}}\}$.

*2) **TA-TSK**:* TA-TSK tries to construct Manchester-like coding in an active slot. Then TA-TSK only backscatters signals in first half or second half time slot in the active time slot. Without loss of generality, we adopt the first half in this paper. Thus, the backscattered symbols vector for TA-TSK is $\mathbf{x}_l \in \{\mathbf{1}_{1\times \mathrm{N}/2}\mathbf{0}_{1\times \mathrm{N}/2}, \mathbf{0}_{1\times \mathrm{N}}\}$.

*3) **FS-TSK**:* FS-TSK backscatters the ambient signals in another frequency that is different from the ambient signal frequency. Specifically, in the active time slot, the tag shifts the ambient signals by toggling its switch in another fixed frequency f_s. The details of the mathematical principle and hardware implementation for frequency shifting can be referred to [40]–[43]. Thus, the strong interference from ambient signals is avoided. The backscattered symbols vector for FS-TSK is $\mathbf{x}_l \in \{e^{j2\pi f_s t}\mathbf{1}_{1\times \mathrm{N}}, \mathbf{0}_{1\times \mathrm{N}}\}$.

A simple illustration of the three TSK schemes is shown in Fig. 2. They all chooses the active slot by the transmission bits based on Tab. II, where $L = 4$. They differ in the backscattered signals in the active slot.

Using the backscattered signal vectors of the three TSK schemes, the received signal vector can be expressed as

$$\mathbf{Y} = [\mathbf{y}_1, \mathbf{y}_2, \cdots \mathbf{y}_L], \tag{4}$$

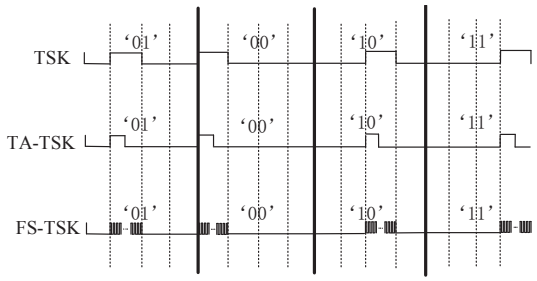

Fig. 2. Examples for the basic TSK, FS-TSK and TA-TSK.

where $\mathbf{y}_l = [y_l(1), y_l(2), \cdots y_l(N)], l = 1, 2, \cdots L$.

III. Detections for Basic TSK, TA-TSK and FS-TSK

We propose the detection algorithms for the three TSK schemes and analyse their performance for complex Gaussian sources and PSK sources in this section.

A. Detections for basic TSK

This subsection discuss the detection for basic TSK and its detection performance.

1) Maximum likelihood detector with training symbols (ML-TS): To use the maximum likelihood (ML) principle, we need to obtain the joint probability density functions (PDFs) of the received signal conditioned on the different active time slot indices and then choose the maximum.

a) CG Source: First, we consider the CG source, and assume $s_l(n) \sim \mathcal{CN}(0, \sigma_s^2)$. Then the received signal vector $\mathbf{y}$ in one time slot is also a complex Gaussian vector. Let $\bar{\mathcal{H}}_0$ and $\bar{\mathcal{H}}_1$ be the hypotheses of $\mathbf{x}_l = \mathbf{0}_{1\times \mathrm{N}}$ and $\mathbf{x}_l = \mathbf{1}_{1\times \mathrm{N}}$. Assuming the channel state information is known, the PDF of $\mathbf{y}_l$ is given by

$$\mathbf{y}_l \sim \begin{cases} \mathcal{CN}(0, \sigma_0^2 \mathbf{I}_N), & \bar{\mathcal{H}}_0, \\ \mathcal{CN}(0, \sigma_1^2 \mathbf{I}_N), & \bar{\mathcal{H}}_1, \end{cases} \tag{5}$$

where $\sigma_0^2 = |h_0|^2\sigma_s^2 + \sigma_w^2$ and $\sigma_1^2 = |h_1|^2\sigma_s^2 + \sigma_w^2$ represent the average powers of the received signals in the two hypotheses. Observing from (5), we know it is unnecessary to obtain the exact channels only σ_0^2 and σ_1^2 are required.

Let $\mathcal{H}_l, l = 1, 2, \cdots, L$ be the hypothesis of the active time slot index. The PDF of $\mathbf{Y}$ under hypothesis $\mathcal{H}_l$ is given by

$$\begin{aligned} \Pr(\mathbf{Y}|\mathcal{H}_l) &= \Pr(\mathbf{y}_l|\bar{\mathcal{H}}_1) \cdot \prod_{l'=1, l'\neq l}^{L} \Pr(\mathbf{y}_{l'}|\bar{\mathcal{H}}_0) \\ &= \frac{\exp\left(-\mathbf{y}_l{}^H (\sigma_1^2 \mathbf{I}_N)^{-1} \mathbf{y}_l\right)}{\pi^N \det(\sigma_1^2 \mathbf{I}_N)} \\ &\quad \cdot \prod_{l'=1, l'\neq l}^{L} \left[\frac{\exp\left(-\mathbf{y}_{l'}{}^H (\sigma_0^2 \mathbf{I}_N)^{-1} \mathbf{y}_{l'}\right)}{\pi^N \det(\sigma_0^2 \mathbf{I}_N)} \right]. \end{aligned} \tag{6}$$

Using the ML principle, the detection rule is given by

$$\hat{l} = \arg\max_l \Pr(\mathbf{Y}|\mathcal{H}_l). \tag{7}$$

Assuming that the reader does not have exact information about h_d, h_b and h_f, the parameters σ_1^2 and σ_0^2 required in (6) need to be calculated using training sequences [1], [23], [24]. At the beginning of transmitting information bits, N_t training symbols have to be sent by the tag. The training symbols vector is $\mathbf{X}_t = [\mathbf{1}_{1\times \mathrm{N}}, \cdots, \mathbf{1}_{1\times \mathrm{N}}, \mathbf{0}_{1\times \mathrm{N}}, \cdots, \mathbf{0}_{1\times \mathrm{N}}]_{1\times N_t N}$, containing $\frac{N_t}{2}$ vectors $\mathbf{1}$ and $\frac{N_t}{2}$ vectors $\mathbf{0}$. The received signal of training symbols is

$$\mathbf{Y}_t = [\mathbf{y}_{t,1}, \mathbf{y}_{t,2}, \cdots \mathbf{y}_{t,N_t}]. \tag{8}$$

Defining the average powers Z_1 and Z_0 as

$$\begin{cases} Z_1 = \frac{2\Sigma||\mathbf{y}_{t,nt}||^2}{N_t}, nt = 1, 2, \cdots, N_t/2, \\ Z_0 = \frac{2\Sigma||\mathbf{y}_{t,nt}||^2}{N_t}, nt = N_t/2 + 1, \cdots, N_t, \end{cases} \tag{9}$$

we have $\hat{\sigma}_1^2 = Z_1$ and $\hat{\sigma}_0^2 = Z_0$.

b) M-PSK Source: We next consider the M-PSK source $s_m(n) = \sqrt{P_s}\exp\left(\frac{2\pi j(m-1)}{M}\right), m = 1, \cdots, M$, where P_s is the average power of the PSK source. Then the PDF of $\mathbf{y}_l$ can be expressed as

$$p(\mathbf{y}_l|\bar{\mathcal{H}}_i) = \prod_{n=1}^{N} \left(\sum_{m=1}^{M} \frac{1}{M} \frac{1}{\pi\sigma_w^2} e^{-\frac{\left|y(n) - h_i\sqrt{P_s}e^{\frac{2\pi j(m-1)}{M}}\right|^2}{\sigma_w^2}} \right). \tag{10}$$

From the PDF of $\mathbf{y}_l$ in (10), we can see that the ML detection cannot be used for the M-PSK source since the exact channel state information h_0 and h_1 are needed but unknown at the reader. We will turn to the energy detection to address this issue.

2) Energy detector with training symbols (ED-TS): The superposition power of the source and the backscatter signals at the active slot is not guaranteed larger than that of the signals at the inactive slots, because the channel coefficients and signals are complex. However, the energy of the active time slot can be either maximum or minimum. If $Z_1 > Z_0$, which means the received signal energy of the active time slot is greater than that of the inactive time slot, the energy of the active time slot is maximum. Otherwise, the energy of the active time slot is minimum. Then the detection rule can be expressed as

$$\begin{cases} I = \arg\max\limits_l \{||\mathbf{y}_1||^2, ||\mathbf{y}_2||^2, \cdots ||\mathbf{y}_L||^2\}, \sigma_1^2 > \sigma_0^2, \\ I = \arg\min\limits_l \{||\mathbf{y}_1||^2, ||\mathbf{y}_2||^2, \cdots ||\mathbf{y}_L||^2\}, \sigma_1^2 < \sigma_0^2. \end{cases} \tag{11}$$

Theorem 1: For basic TSK with a CG source, the ML detection is equivalent to the ED detection for AmBC.

Proof: See Appendix A.

3) BER analysis for ED-TS: There are three detection cases in (11) for the two sources and the performance analysis will be elaborated respectively. The analysis in *Case 1* and *Case 2* is conducted for the CG source while the analysis for PSK sources is presented in *Case 3*.

Case 1 ($\sigma_1^2 > \sigma_0^2$ under CG sources):

Theorem 2: The BER in this case is given by

$$P_{SER} = \frac{2^{\log_2(L)-1}}{L-1} \frac{1}{\sigma_1^{2N}\Gamma(N)} \sum_{l=1}^{L-1} (-1)^{l-1} \binom{L-1}{l} \times \sum_{\sum_{n=0}^{N-1} k_n = l} \frac{l!}{\prod_{n=0}^{N-1} k_n! (\sigma_0^{2n} n!)^{k_n}} \frac{\Gamma(1+a)}{b^{1+a}}. \tag{12}$$

Proof : See Appendix B.

Case 2 ($\sigma_1^2 < \sigma_0^2$ under CG sources):

Theorem 3: The BER of this case is given by

$$P_{BER} = \frac{2^{\log_2(L)-1}}{L-1} \frac{1}{\sigma_0^{2N}\Gamma(N)} \sum_{l=1}^{L-1} (-1)^{l-1} \binom{L-1}{l} \times \sum_{\sum_{n=0}^{N-1} k_n = l} \frac{l!}{\prod_{n=0}^{N-1} k_n! (\sigma_1^{2n} n!)^{k_n}} \frac{\Gamma(1+a)}{b^{1+a}}. \tag{13}$$

Proof: See Appendix C.

With the analysis in *Case 1* and *Case 2*, the final P_{BER} expression can be obtained by integrating (12) and (13) into one

$$P_{BER} = \frac{2^{\log_2(L)-1}}{L-1} \frac{1}{\sigma_{max}^{2N}\Gamma(N)} \sum_{l=1}^{L-1} (-1)^{l-1} \binom{L-1}{l} \times \sum_{\sum_{n=0}^{N-1} k_n = l} \frac{l!}{\prod_{n=0}^{N-1} k_n! (\sigma_{min}^{2n} n!)^{k_n}} \frac{\Gamma(1+a)}{b^{1+a}}, \tag{14}$$

where $\sigma_{max}^2 = \max\{\sigma_1^2, \sigma_0^2\}$, and $\sigma_{min}^2 = \min\{\sigma_1^2, \sigma_0^2\}$.

Case 3 (under PSK sources): In *Case 3*, both cases of $\sigma_1^2 > \sigma_0^2$ and $\sigma_1^2 < \sigma_0^2$ are included. Considering PSK source, Z_l and Z_{l_a} are the non-central chi-squared distribution with $2N$ DoF. Their non-central parameters are $N|h_0|^2 P_s$ and $N|h_1|^2 P_s$ respectively. However, the PDF expression of non-central chi-squared distribution is too complicated to acquire a closed-form result. To obtain a tractable result, we investigate the BER of PSK sources with a large N and $L = 2$. When $L = 2$, TSK equals Manchester code. In this situation, Z_l and Z_{l_a} can be appropriated as the normal distribution. The PDFs are listed as follows

$$\begin{cases} f_{Z_{l_a}}(z) = \mathcal{N}(N\sigma_1^2, 2N|h_1|^2 P_s \sigma_w^2 + N\sigma_w^4), \\ f_{Z_l}(z) = \mathcal{N}(N\sigma_0^2, 2N|h_0|^2 P_s \sigma_w^2 + N\sigma_w^4), l \neq l_a. \end{cases} \tag{15}$$

Then, the BER can be obtained by [24]

$$P_{BER} = \frac{1}{2} erfc\left(\frac{\sqrt{N}\left||h_1|^2 - |h_0|^2\right|}{2\sqrt{\frac{|h_1|^2+|h_0|^2}{\gamma} + \frac{1}{\gamma^2}}} \right), \tag{16}$$

where $\gamma = P_s/\sigma_w^2$.

4) Energy detector without training symbols (ED-NoTS): We notice that the inactive slot often has an energy neither the maximum nor the minimum among all the slots. In this sense, the inactive signals can be considered as the training symbols, removing the necessity of dedicated training symbols. In this case, the maximum/minimum signal energy can be obtained by

$$\begin{cases} Z_{max} = \max\{||\mathbf{y}_1||^2, ||\mathbf{y}_2||^2, \cdots ||\mathbf{y}_L||^2\}, \\ Z_{min} = \min\{||\mathbf{y}_1||^2, ||\mathbf{y}_2||^2, \cdots ||\mathbf{y}_L||^2\}, \end{cases} \tag{17}$$

and l_{max} and l_{min} are the corresponding indices to the Z_{max} and Z_{min}. Then, the active time slot is detected by

$$\sum_{l=1, l\neq l_{min}, l\neq l_{\max}}^{L} \left|Z_{max} - ||\mathbf{y}_l||^2\right| \underset{l_{\min}}{\overset{l_{\max}}{\gtrless}} \sum_{l=1, l\neq l_{min}, l\neq l_{\max}}^{L} \left|Z_{\min} - ||\mathbf{y}_l||^2\right|. \tag{18}$$

As shown in (18), we can conclude that this detector needs at least 4 time slots. Actually, the detection in (18) is a distance based detector and we choose the time slot which has maximum distance to other time slots as the active time slot.

B. Detection for TA-TSK

1) Energy detection for TA-TSK: Different from the basic TSK, TA-TSK only activates half of a time slot. To determine the index of the active time slot, the straightforward method is to calculate the energy difference within one time slot and choose the maximum one among all time slots as the active time slot. However, the channel coherent time is unknown and channel gains in different time slots may not be the same. Thus, the maximum of the energy differences cannot reflect the true active time slot. To address this issue, the maximum of the relative energy difference is used to determine the active time slot index.

We define the relative energy difference as the ratio of the energy difference in a slot to a reference energy, which is assumed to be the minimum energy in a slot. Thus, the detection rule can be expressed as

$$\hat{l} = \arg\max_l \frac{\left| \sum_{n=1}^{N/2} |y_l(n)|^2 - \sum_{n=N/2+1}^{N} |y_l(n)|^2 \right|}{\min\left\{ \sum_{n=1}^{N/2} |y_l(n)|^2, \sum_{n=N/2+1}^{N} |y_l(n)|^2 \right\}}. \tag{19}$$

When the channel is static, the active time slot can be identified by the following simplified equation

$$\hat{l} = \arg\max_l \left| \sum_{n=1}^{N/2} |y_l(n)|^2 - \sum_{n=N/2+1}^{N} |y_l(n)|^2 \right|. \tag{20}$$

This is because the denominator in (19) is the same in the static channel scenario.

2) BER analysis for TA-TSK: The BER analysis of TA-TSK under the detection by (19) is intractable. We turn to obtain the BER under the detection by (20). We also discuss two sources for TA-TSK.

a) CG sources: A detection error occurs when the energy difference of at least one non-active time slot is greater than that of the active time slot. Mathematically, the SER can be expressed as

$$P_{SER} = 1 - \Pr\{\Delta Z'_{l_a} \geq \Delta Z'_{\max}\}, \tag{21}$$

where $\Delta Z'_{\max} = \max\{\Delta Z'_l\}, l = 1, 2, \cdots L, l \neq l_a$, $\Delta Z'_l = \left|\sum_{n=1}^{N/2} |y_l(n)|^2 - \sum_{n=N/2+1}^{N} |y_l(n)|^2\right|, l = 1, 2, \cdots, L$.

The sum of the received signals follows the chi-square distribution. However, this distribution is complicated. To obtained a tractable solution, we approximate it by Gaussian distribution when N is large. Thus, the approximated PDFs of the received signal energy under the CG source are given as follows

$$\begin{cases} \sum\limits_{n=1}^{N/2} |y_{l_a}(n)|^2 \sim \mathcal{N}\left(\frac{N\sigma_1^2}{2}, \frac{N\sigma_1^4}{2}\right), l = l_a, \\ \sum\limits_{n=1}^{N/2} |y_l(n)|^2 \sim \mathcal{N}\left(\frac{N\sigma_0^2}{2}, \frac{N\sigma_0^4}{2}\right), l = 1,2, \cdots L, l \neq l_a, \\ \sum\limits_{n=N/2+1}^{N} |y_l(n)|^2 \sim \mathcal{N}\left(\frac{N\sigma_0^2}{2}, \frac{N\sigma_0^4}{2}\right), l = 1, 2, \cdots L. \end{cases} \tag{22}$$

Thus, the PDF of the energy difference in the active time slot is derived as

$$\begin{aligned} &\sum_{n=1}^{N/2} |y_{l_a}(n)|^2 - \sum_{n=N/2+1}^{N} |y_{l_a}(n)|^2 \\ &\sim \mathcal{N}\left(\frac{N\sigma_1^2 - N\sigma_0^2}{2}, \frac{N\sigma_1^4 + N\sigma_0^4}{2}\right) = \mathcal{N}\left(\mu_{\Delta Z'_{l_a}}, \sigma^2_{\Delta Z'_{l_a}}\right). \end{aligned} \tag{23}$$

Similarly, the PDF of energy difference in the inactive time slot is

$$\begin{aligned} &\sum_{n=1}^{N/2} |y_l(n)|^2 - \sum_{n=N/2+1}^{N} |y_l(n)|^2 \sim \mathcal{N}\left(0, N\sigma_0^4\right) \\ &= \mathcal{N}\left(\mu_{\Delta Z'_l}, \sigma^2_{\Delta Z'_l}\right), l = 1, 2, \cdots L, l \neq l_a. \end{aligned} \tag{24}$$

The PDF of $\Delta Z'_{l_a}$ is derived as

$$\begin{aligned} \Delta Z'_{l_a} \sim &\frac{1}{\sqrt{2\pi\sigma^2_{\Delta Z'_{l_a}}}} \exp\left(-\frac{(\Delta Z'_{l_a} + \mu_{\Delta Z'_{l_a}})^2}{2\sigma^2_{\Delta Z'_{l_a}}}\right) \\ &+ \frac{1}{\sqrt{2\pi\sigma^2_{\Delta Z'_{l_a}}}} \exp\left(-\frac{(\Delta Z'_{l_a} - \mu_{\Delta Z'_{l_a}})^2}{2\sigma^2_{\Delta Z'_{l_a}}}\right), \Delta Z'_{l_a} \geq 0, \end{aligned} \tag{25}$$

and the PDF of $\Delta Z'_l$, $l = 1, 2, \cdots L, l \neq l_a$ is

$$\Delta Z'_l \sim \frac{2}{\sqrt{2\pi\sigma^2_{\Delta Z'_l}}} \exp\left(-\frac{(\Delta Z'_l)^2}{2\sigma^2_{\Delta Z'_l}}\right), \Delta Z'_l \geq 0, \tag{26}$$

The CDF of $\Delta Z'_l$ is

$$F_{\Delta Z'_l}(z) = 1 - 2Q\left(\frac{\Delta Z'_l}{\sigma_{\Delta Z'_l}}\right), \tag{27}$$

where $Q(x) = \int_x^{+\infty} \frac{1}{\sqrt{2\pi}} \exp(-t^2/2) dt$. The SER can be obtained by

$$P_{SER} = 1 - \int_0^{+\infty} f_{\Delta Z'_{l_a}}(z) F^{L-1}_{\Delta Z'_l}(z) dz. \tag{28}$$

Substituting (25) and (26) into (28), the P_{SER} becomes (29) as shown at the top of next page. The integral in (29) is hard to obtain its closed-form result due to its complexity. We will analyse its numerical results in Sec. IV.

TA-TSK signals are uniformly distributed in the possible time slots. Then the corresponding BER can be obtained as [46]

$$P_{BER} = \frac{2^{\log_2(L)-1}}{L-1} P_{SER}. \tag{30}$$

b) PSK sources: We investigate the BER of TA-TSK with PSK sources. The PDFs of the received signal energy under the PSK sources similar to (15) are listed as follows

$$\begin{cases} \sum\limits_{n=1}^{N/2} |y_{l_a}(n)|^2 \sim \mathcal{N}\left(\frac{N\sigma_1^2}{2}, N|h_1|^2 P_s \sigma_w^2 + \frac{N\sigma_w^4}{2}\right), \\ \sum\limits_{n=1}^{N/2} |y_l(n)|^2 \sim \mathcal{N}\left(\frac{N\sigma_0^2}{2}, N|h_0|^2 P_s \sigma_w^2 + \frac{N\sigma_w^4}{2}\right), l \neq l_a, \\ \sum\limits_{n=N/2+1}^{N} |y_l(n)|^2 \sim \mathcal{N}\left(\frac{N\sigma_0^2}{2}, N|h_0|^2 P_s \sigma_w^2 + \frac{N\sigma_w^4}{2}\right). \end{cases} \tag{31}$$

Substituting (31) into (23)-(30), we can readily get the BER for TA-TSK under PSK sources.

C. Detection for FS-TSK

1) Energy detection for FS-TSK: Assume that the reader is capable of removing the direct interference, i.e., the reader is equipped with a band-pass filter, and the ambient signal can be filtered out. In multiple frequency shift keying (MFSK) [35], the tag conveys its information by shifting the backscattered signals to multiple frequency bands. Then the receiver needs to monitor all the shifted frequency bands using multiple band-pass filters to detect the backscattered signals. Our FS-TSK method shifts the backscattered signals to only one fixed frequency band. Thus it requires only one frequency band and one band-pass filter at the receiver as shown in Fig. 3. As the the direct link signals are filtered out, the baseband received signal can be expressed by

$$\begin{cases} y_l(n) = h_b h_f \alpha x_l(n) s_l(n) + w_l(n), l = l_a, \\ y_l(n) = w_l(n), \qquad\qquad\qquad\quad l \neq l_a. \end{cases} \tag{32}$$

The energy detection rule can be derived as

$$\hat{l} = \arg\max_l ||\mathbf{y}_l||^2. \tag{33}$$

2) BER analysis: Since the direct interference has been removed in FS-TSK, the corresponding parameters of σ_1^2 and σ_0^2 have been changed to $\sigma^2_{fs,0} = \sigma_w^2$ and $\sigma^2_{fs,1} = |\alpha h_b h_f|^2 \sigma_s^2 + \sigma_w^2$. We only need to consider the case of $\sigma^2_{fs,1} > \sigma^2_{fs,0}$ when calculating the BER of FS-TSK. The BER calculation process of FS-TSK follows similar steps in Sec. III-A3. We omit specific derivation process here for brevity and show the final result in the following

$$\begin{aligned} P_{SER} = &\frac{2^{\log_2(L)-1}}{L-1} \frac{1}{\sigma^{2N}_{fs,1}\Gamma(N)} \sum_{l=1}^{L-1} (-1)^{l-1} \binom{L-1}{l} \\ &\times \sum_{\sum_{n=0}^{N-1} k_n = l} \frac{l!}{\prod_{n=0}^{N-1} k_n! (\sigma^{2n}_{fs,0} n!)^{k_n}} \frac{\Gamma(1+a)}{b'^{1+a}}, \end{aligned} \tag{34}$$

$$P_{SER} = 1 - \int_0^{+\infty} \left[\frac{1}{\sqrt{2\pi\sigma^2_{\Delta Z'_{la}}}} \exp\left(-\frac{(z+\mu_{\Delta Z'_{la}})^2}{2\sigma^2_{\Delta Z'_{la}}} \right) + \frac{1}{\sqrt{2\pi\sigma^2_{\Delta Z'_{la}}}} \exp\left(-\frac{(z-\mu_{\Delta Z'_{la}})^2}{2\sigma^2_{\Delta Z'_{la}}} \right) \right] \left[1 - 2Q\left(\frac{z}{\sigma_{\Delta Z'_l}} \right) \right]^{L-1} dz. \quad (29)$$

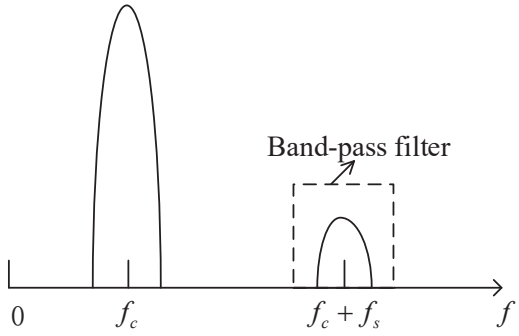

Fig. 3. Illustration of shifted frequency spectrum. The value f_c is the center frequency of the source signal, f_s is the switching frequency and $f_c + f_s$ is the frequency of the backscattered signal in the active time slot.

where $b' = \frac{1}{\sigma^2_{fs,1}} + \frac{l}{\sigma^2_{fs,0}}$. Note that based on (34), our proposed FS-TSK has the same detection performance compared with the proposed MFSK in [35].

IV. Simulation Results and Discussions

In this section, simulation results are presented to evaluate the performance of the proposed schemes.

A. Parameter Settings

We set $h_d \sim \mathcal{CN}(0,2)$, $h_b, h_f \sim \mathcal{CN}(0,1)$. The coefficient α representing the scattering efficiency and antenna gain is 0.5. The source power σ_s^2 and P_s are assumed equal and are set to 1. The number of training symbols is set as $N_t = 14$. Without loss of generality, the type of the M-PSK source is the 8PSK source. The bit signal-to-noise ratio (b-SNR) is defined as $\frac{\sigma_s^2}{\sigma_w^2 log_2 L}$.

B. Performance Discussions

1) Impact of b-SNR on BER: We first study the BER of different detectors under different b-SNR. The parameter N is set to 80 for both the CG source and the PSK source. To provide a BER benchmark performance, we compare TSK with OOK proposed in [23]. The length of the training sequence used in [23] is set as 14 and is the same as TSK.

From Fig. 4, the BER decreases with the increase of b-SNR. But the BER has an error floor because the interference from the direct link also increases in the high b-SNR regime. The proposed TSK with $L = 2$ has almost the same BER performance as OOK for CG sources. Our TSK with $L = 2$ can be considered as Manchester code and the similar performance has been observed in [24]. According to the analysis in Sec. III-A2, the BERs of ML-TS and ED-TS are the same with perfect channel state information. However, due to the

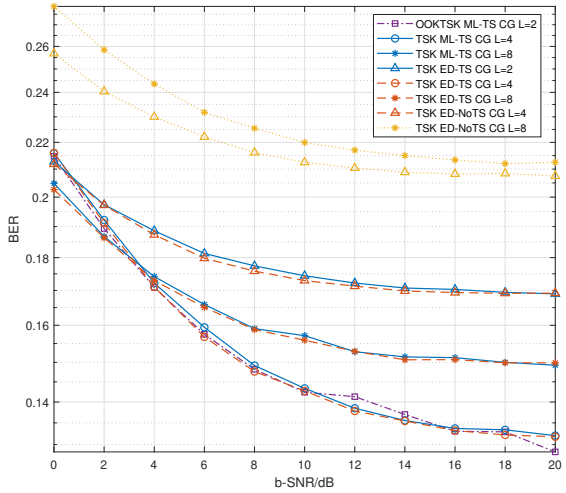

Fig. 4. BER versus b-SNR for the CG source

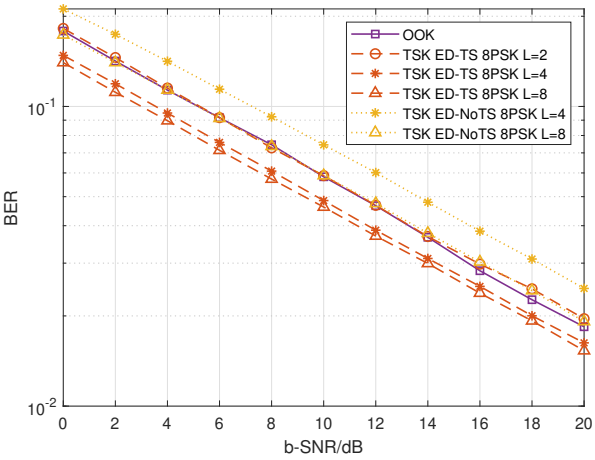

Fig. 5. BER versus b-SNR for the 8PSK source

estimated parameters $\hat{\sigma}_1^2$ and $\hat{\sigma}_0^2$ used at both ML-TS and ED-TS, the BER of the ML-TS detection is close to the BER of ED-TS but not the same as shown in Fig. 4. ED-TS has a lower BER than ED-NoTS at the cost of sending training sequence. Increasing the modulation order of TSK cannot bring benefits to CG sources in the high b-SNR regime under the ED-TS detection, while the high-order TSK decreases the BER across all b-SNR regime under the NoTS-ED detection.

Similarly, the proposed TSK with $L = 2$ has almost the same BER performance as OOK for PSK sources. As shown in Fig. 5, we can see that the larger L leads to the better BER performance under the 8-PSK source. This indicates that

the high-order TSK is suitable for PSK sources. Due to the constant envelope of PSK sources, BER with PSK sources is lower than that with CG sources and there is no error floor with PSK sources. With the increase of modulation order L, the gap between the BER curves narrows under the ED-TS detection. Therefore, the BER gain by increasing the modulation order L becomes smaller.

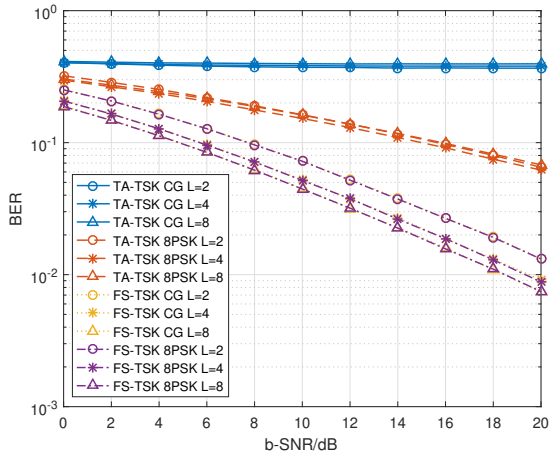

Fig. 6. BER versus b-SNR for TA-TSK and FS-TSK under fast fading channels

We subsequently study the b-SNR versus the BER of TA-TSK and FS-TSK in the fast fading channels. We set the channel coherent time to one time slot. From Fig. 6, we can see the BER of TA-TSK is lager than FS-TSK. This is because FS-TSK eliminates the direct link interference (DLI). Also, without DLI, FS-TSK with CG sources and PSK sources achieves almost the same BER. But for TA-TSK, there is a huge BER gap between CG sources and PSK sources. It is noted that the 4-order TA-TSK has a better BER performance than other modulation orders. As for FS-TSK, the higher order leads to the lower BER because of no DLI at the receiver.

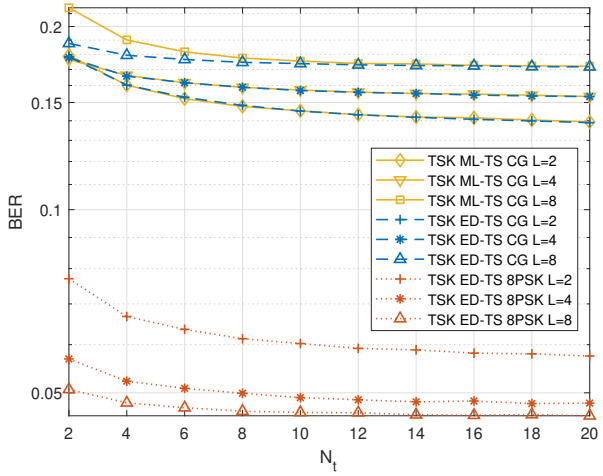

Fig. 7. BER versus N_t.

2) Impact of N_t and N on BER: The impact of the length of the training sequence on BER is illustrated in Fig. 7. The SNR is set as 10 *dB*. We can see that the increase of the training sequence length leads to the decrease of the BER from Fig. 7, but the BER will be saturated in high SNR. We cannot keep increasing the length of the training sequence to reduce the BER. For both CG and PSK sources, 12 training symbols are sufficient to achieve almost the lowest BER.

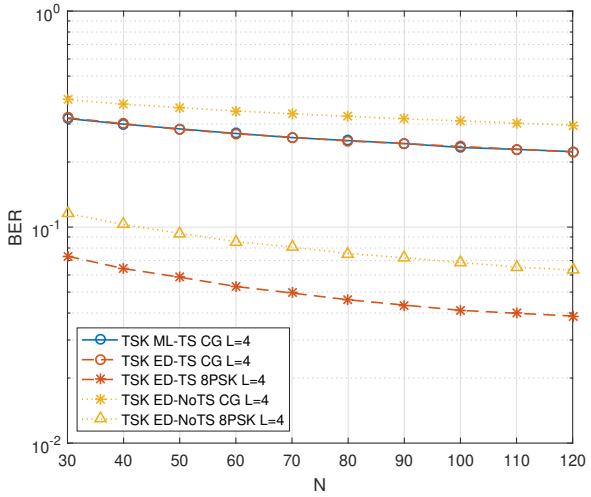

Fig. 8. BER versus N

We next study the impact of the length of the received signal vector N in one time slot on BER. It is obvious that a larger N results in a smaller BER for all detectors, and there is no error floor in the large N region as shown in Fig. 8. To decrease the BER continuously, the tag can extend the duration of the backscattered symbol.

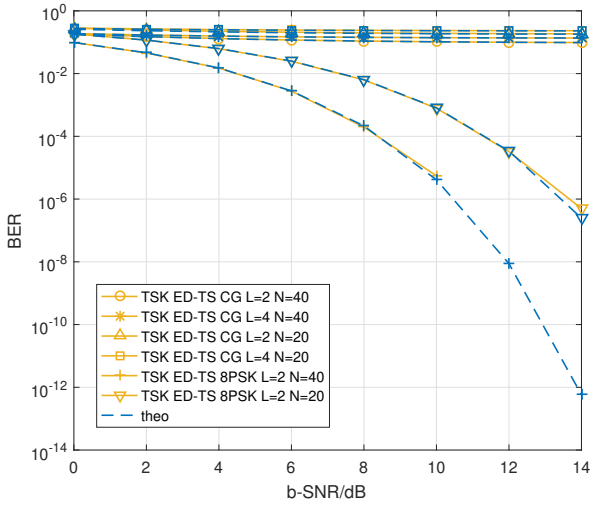

Fig. 9. BER versus b-SNR for TSK

3) Verification of the theoretical analysis: The b-SNR versus the BER of TSK is illustrated in Fig. 9. We can see the

theoretical BER agrees with the BER of simulations, validating the correctness of the theoretical analysis.

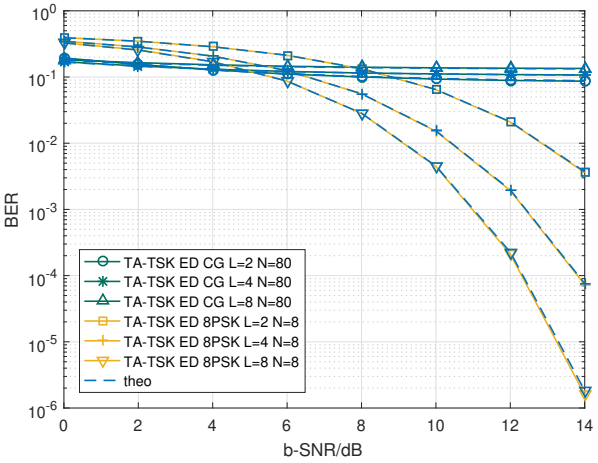

Fig. 10. BER versus b-SNR for TA-TSK

The detection BER of TA-TSK under the static channel scenario in different b-SNR is studied in Fig. 10. The theoretical BERs are consistent with the BERs of simulations, verifying that the theoretical analysis is correct.

V. Conclusion

This paper has proposed three TSK modulation schemes, i.e., basis TSK, TA-TSK, and FS-TSK, to achieve high order modulation in the time domain for AmBC. Detection methods with and without training symbols are studied for the three TSK schemes. Simulation results show that the high-order TSK with training symbols is beneficial to the M-PSK modulated source signal while is not for the CG source. For TA-TSK, a high modulation order can decrease the BER under M-PSK sources. FS-TSK removes the direct link interference and the BERs under M-PSK and CG sources are almost the same. Moreover, a high modulation order can decrease the BER for both sources with FS-TSK.

Appendix A
Proof of Theorem 1

From the ML detection in (6), we have

$$\begin{aligned}
&\max_{l} \frac{\exp\left(-\mathbf{y}_l{}^H(\sigma_1^2\mathbf{I}_N)^{-1}\mathbf{y}_l\right)}{\pi^N \det(\sigma_1^2\mathbf{I}_N)} \cdot \prod_{l'=1,l'\neq l}^{L}\left[\frac{\exp\left(-\mathbf{y}_{l'}{}^H(\sigma_0^2\mathbf{I}_N)^{-1}\mathbf{y}_{l'}\right)}{\pi^N \det(\sigma_0^2\mathbf{I}_N)}\right] \\
&\Rightarrow \max_{l} \exp\left(-\mathbf{y}_l{}^H(\sigma_1^2\mathbf{I}_N)^{-1}\mathbf{y}_l - \sum_{l'=1,l'\neq l}^{L}\mathbf{y}_{l'}{}^H(\sigma_0^2\mathbf{I}_N)^{-1}\mathbf{y}_{l'}\right) \\
&\Rightarrow \max_{l} \exp\left(-\frac{||\mathbf{y}_l||^2}{\sigma_1^2} - \sum_{l'=1,l'\neq l}^{L}\frac{||\mathbf{y}_{l'}||^2}{\sigma_0^2}\right) \\
&\Rightarrow \max_{l} \exp\left(-\frac{\sigma_0^2||\mathbf{y}_l||^2 + \sum_{l'=1,l'\neq l}^{L}\sigma_1^2||\mathbf{y}_{l'}||^2}{\sigma_0^2\sigma_1^2}\right) \\
&\Rightarrow \min_{l} \ \sigma_0^2||\mathbf{y}_l||^2 + \sum_{l'=1,l'\neq l}^{L}\sigma_1^2||\mathbf{y}_{l'}||^2.
\end{aligned} \tag{35}$$

We can detect l by

$$\sigma_0^2||\mathbf{y}_l||^2 + \sum_{\tilde{l}=1,\tilde{l}\neq l}^{L}\sigma_1^2||\mathbf{y}_{\tilde{l}}||^2 \underset{l}{\overset{l'}{\gtrless}} \sigma_0^2||\mathbf{y}_{l'}||^2 + \sum_{\tilde{l}=1,\tilde{l}\neq l'}^{L}\sigma_1^2||\mathbf{y}_{\tilde{l}}||^2. \tag{36}$$

Removing the same terms on both sides, we get

$$\sigma_0^2\left(||\mathbf{y}_l||^2 - ||\mathbf{y}_{l'}||^2\right) \underset{l}{\overset{l'}{\gtrless}} \sigma_1^2\left(||\mathbf{y}_l||^2 - ||\mathbf{y}_{l'}||^2\right). \tag{37}$$

As both $\sigma_1^2 > 0$ and $\sigma_0^2 > 0$, we discuss (37) in two cases.

- $\sigma_1^2 > \sigma_0^2$: In this case, to make the right decision l in (37), $||\mathbf{y}_l||^2 - ||\mathbf{y}_{l'}||^2 > 0$ should be satisfied, which means the signal energy in the inactive time slot is smaller than that in the active time slot.
- $\sigma_1^2 < \sigma_0^2$: If $\sigma_1^2 < \sigma_0^2$, to make the correct detection l in (37), $||\mathbf{y}_l||^2 - ||\mathbf{y}_{l'}||^2 < 0$ is needed, which means the signal energy in the active time slot is smaller than that in the inactive time slot.

Since l' represents any inactive time slot index, this decision rule in (37) can be rewritten as (11). The activated time slot index is determined by choosing the maximum energy value or the minimum energy value according to the channel conditions. Thus, the ML detection is the same as the energy detection.

Appendix B
Proof of Theorem 2

In this case, the energy of the active time slot is maximum and a judgment error occurs when the energy of at least one non-active time slot is greater than the energy of the active time slot. Mathematically, the symbol error rate (SER) can be obtained by

$$P_{SER} = 1 - \Pr\{Z_{l_a} \geq Z'_{max}\}, \tag{38}$$

where $Z'_{max} = \max\{Z_l\}, l = 1, 2, \cdots L, l \neq l_a$, l_a is the active time slot index, $Z_l = \sum_{n=1}^{N}|y_l(n)|^2$.

With CG sources, Z_l and Z_{l_a} are the sum of $2N$ $i.i.d.$ Gaussian variables, so Z_l and Z_{l_a} follow the χ^2_{2N} distribution with PDF as follows

$$\begin{cases} f_{Z_l}(z) = \frac{z^{N-1}e^{-\frac{z}{\sigma_0^2}}}{\sigma_0^{2N}\Gamma(N)}, z > 0, l = 1, 2, \cdots L, l \neq l_a, \\ f_{Z_{l_a}}(z) = \frac{z^{N-1}e^{-\frac{z}{\sigma_1^2}}}{\sigma_1^{2N}\Gamma(N)}, z > 0. \end{cases} \tag{39}$$

Since Z_l is an $i.i.d.$ random variable, the cumulative distribution function (CDF) of Z'_{max} can be expressed as

$$F_{Z'_{max}}(z) = \Pr\{Z'_{max} < z\} = P^{L-1}(z), \tag{40}$$

where

$$P(z) = \Pr\{Z_l \leq z\} = 1 - \frac{\Gamma\left(N, \frac{z}{\sigma_0^2}\right)}{\Gamma(N)}. \tag{41}$$

Using the binomial expansion theorem, we obtain

$$F_{Z'_{max}}(z) = 1 - \sum_{l=1}^{L-1}(-1)^{l-1}\binom{L-1}{l}\left[\frac{\Gamma\left(N, \frac{z}{\sigma_0^2}\right)}{\Gamma(N)}\right]^l. \tag{42}$$

Next, the SER of the system can be derived as

$$\begin{aligned} P_{SER} &= 1 - \int_0^{+\infty} f_{Z_{l_a}}(z) F_{Z'_{max}}(z) dz \\ &= \frac{1}{\sigma_1^{2N}\Gamma(N)} \sum_{l=1}^{L-1} (-1)^{l-1} \binom{L-1}{l} \\ &\times \underbrace{\int_0^{+\infty} z^{N-1} e^{-\frac{z}{\sigma_1^2}} \left[\frac{\Gamma\left(N, \frac{z}{\sigma_0^2}\right)}{\Gamma(N)} \right]^l dz}_{I_1}. \end{aligned} \tag{43}$$

It is hard to evaluate I_1 directly because of the presence of incomplete gamma function with $l(>1)$ power. Instead, we expand the incomplete gamma function by using the following relationship [45, eqs. 8.2.4, 8.4.10, and 8.4.11]

$$\frac{\Gamma(N,x)}{\Gamma(N)} = Q(N,x), \tag{44}$$

$$Q(N,x) = \sum_{n=0}^{N-1} \frac{x^n}{n!} e^{-x}. \tag{45}$$

The integral I_1 can then be expressed as follows

$$I_1 = \int_0^{+\infty} z^{N-1} e^{-\frac{z}{\sigma_1^2}} \left[\sum_{n=0}^{N-1} \frac{\left(\frac{z}{\sigma_0^2}\right)^n}{n!} e^{-\frac{z}{\sigma_0^2}} \right]^l dz. \tag{46}$$

Then, utilizing the following polynomial expansion identity [44]

$$\left(\sum_{n=0}^{N-1} x_n \right)^l = \sum_{\sum_{n=0}^{N-1} k_n = l} \frac{l!}{\prod_{n=0}^{N-1} k_n!} \prod_{n=0}^{N-1} x_n^{k_n}, \quad k_n \in \mathbb{N}, \tag{47}$$

we further obtain

$$I_1 = \sum_{\sum k_n = l} \frac{l!}{\prod_{n=0}^{N-1} k_n! (\sigma_0^{2n} n!)^{k_n}} \int_0^{+\infty} z^a e^{-bz} dz, \tag{48}$$

where $a = N - 1 + \sum_{n=0}^{N-1} n k_n, b = \frac{1}{\sigma_1^2} + \frac{l}{\sigma_0^2}$.

Applying the following integration relationship [45, eq. 3.351.3]

$$\int_0^{+\infty} z^a e^{-bz} dz = \frac{\Gamma(1+a)}{b^{1+a}}, \tag{49}$$

we obtain the final expression as

$$\begin{aligned} P_{SER} &= \frac{1}{\sigma_1^{2N}\Gamma(N)} \sum_{l=1}^{L-1} (-1)^{l-1} \binom{L-1}{l} \\ &\times \sum_{\sum_{n=0}^{N-1} k_n = l} \frac{l!}{\prod_{n=0}^{N-1} k_n! (\sigma_0^{2n} n!)^{k_n}} \frac{\Gamma(1+a)}{b^{1+a}}, \end{aligned} \tag{50}$$

where $\sum_{n=0}^{N-1} k_n = l, k_n \in \mathbb{N}$. Assuming that s_0 corresponds to the transmission bit sequence of length $\log_2(L)$ with a "0" at the first component. Due to the symmetry of the constellation for orthogonal TSK, when s_0 is sent, the probabilities of receiving other signals of $s_l, l = 2, \cdots, L$ are equal. Therefore, for any $l = 2, \cdots, L$,

$$P[s_l \text{ received} | s_0 \text{ sent}] = \frac{P_{SER}}{L-1}. \tag{51}$$

The error probability at the first component of s_0 is the probability of detecting an s_l corresponding a sequence with a "1" at the first component. Since there are $2^{\log_2(L)-1}$ such transmission sequences, the average BER is given by [46]

$$P_{BER} = \frac{2^{\log_2(L)-1}}{L-1} P_{SER}. \tag{52}$$

Finally, substituting (50) into (52), (12) can be obtained.

Appendix C
Proof of Theorem 3

In this case, the energy of the active time slot is minimum and a judgment error occurs when the energy of at least one non-active time slot is less than the energy of the active time slot. Mathematically, the SER can be expressed as

$$P_{SER} = 1 - \Pr\{Z_{l_a} < Z'_{\min}\}, \tag{53}$$

where $Z'_{min} = \min\{Z_l\}, l = 1, 2, \cdots L, l \neq l_a$. Further, the SER can be calculated by

$$P_{SER} = 1 - \Pr\{-Z_{l_a} \geq Z^*_{max}\}, \tag{54}$$

where $Z^*_{max} = \max\{-Z_l\}, l = 1, 2, \cdots L, l \neq l_a$. The PDFs of $-Z_l$ and $-Z_{l_a}$ follow

$$\begin{cases} f_{-Z_{l_a}}(z) = \frac{(-z)^{N-1} e^{\frac{z}{\sigma_1^2}}}{\sigma_1^{2N}\Gamma(N)}, z < 0, \\ f_{-Z_l}(z) = \frac{(-z)^{N-1} e^{\frac{z}{\sigma_0^2}}}{\sigma_0^{2N}\Gamma(N)}, z < 0, l = 1, 2, \cdots L, l \neq l_a. \end{cases} \tag{55}$$

The following calculation process is similar to (40)-(51) in *Case 1*, so omitted here for brevity.

References

[1] J. Chen, H. Yu, Q. Guan, and W. Chen, "High-order time shift keying modulation and detection for ambient backscatter communications," in *Proc. IEEE ICCC Workshops*, Dalian, China, pp. 1–6 , Sep. 2023.

[2] D. T. Hoang, D. Niyato, D. I. Kim, N. Van Huynh, and S. Gong, *Ambient Backscatter Communication Networks*. Cambridge, U.K.: Cambridge Univ. Press, Apr. 2020.

[3] D. A. Loku Galappaththige, F. Rezaei, C. Tellambura, and S. Herath, "Link budget analysis for backscatter-based passive IoT," *IEEE Access*, vol. 10, pp. 128890–128922, 2022.

[4] F. Rezaei, D. Galappaththige, C. Tellambura, and S. Herath, "Coding techniques for backscatter communications—A contemporary survey," *IEEE Commun. Surveys Tut.*, vol. 25, no. 2, pp. 1020–1058, 2nd Quart. 2023.

[5] B. Gu, D. Li, H. Ding, G. Wang and C. Tellambura,"Breaking the Interference and Fading Gridlock in Backscatter Communications: State-of-the-Art, Design Challenges, and Future Directions," *IEEE Commun. Surveys Tut.*, early access, 2024.

[6] D. K. Klair, K.-W. Chin, and R. Raad, "A survey and tutorial of RFID anti-collision protocols," *IEEE Commun. Surveys Tuts.*, vol. 12, no. 3, pp. 400–421, 3rd Quart., 2010.

[7] J. Kimionis, A. Bletsas, and J. N. Sahalos, "Increased range bistatic scatter radio," *IEEE Trans. Commun.*, vol. 62, no. 3, pp. 1091–1104, Mar. 2014.

[8] D. Li, "Two birds with one stone: Exploiting decode-and-forward relaying for opportunistic ambient backscattering," *IEEE Trans. Commun.*, vol. 68, no. 3, pp. 1405-1416, Mar. 2020.

[9] D. Li,"Hybrid active and passive antenna selection for backscatter-assisted MISO systems," *IEEE Trans. Commun.*, vol. 68, no. 11, pp. 7258-7269, Nov. 2020.

[10] V. Liu, A. Parks, V. Talla, S. Gollakota, D. Wetherall, and J. R. Smith, "Ambient backscatter: Wireless communication out of thin air," in *Proc. ACM SIGCOMM*, Hong Kong, China, pp. 39-50, Jun. 2013.

[11] A. Wang, V. Iyer, V. Talla, J. R. Smith, and S. Gollakota, "FM backscatter: Enabling connected cities and smart fabrics," in *Proc. 14th USENIX Symp. Netw. Syst. Design Implement. (NSDI)*, Boston, MA, USA, pp. 243–258, 2017.

[12] K. Xu, W. Gong, Y. Li, J. M. Purushothama, G. Goussetis, S. McLaughlin, J. S. Thompson, C. Song and Y. Ding, "FM rider: Two-FSK modulation-based ambient FM backscatter over 100 m distance," *IEEE Trans. Microw. Theory Techn.*, early access, pp. 1-13, Feb, 2024.

[13] B. Kellogg, A. Parks, S. Gollakota, J. R. Smith and D. Wetherall, "Wi-Fi backscatter: Internet connectivity for RF-powered devices," in *Proc. ACM SIGCOMM*, Chicago, IL, USA, pp. 607-618, Aug. 2014.

[14] A. Abedi, F. Dehbashi, M. H. Mazaheri, O. Abari and T. Brecht, "WiTAG: Seamless WiFi backscatter communication," in *Proc. ACM SIGCOMM*, Virtual Event, NY, USA, pp. 240-252, Jul. 2020.

[15] X. He, W. Jiang, M. Cheng, X. Zhou, P. Yang, and B. Kurkoski, "Guardrider: Reliable WiFi backscatter using Reed-Solomon codes with QoS guarantee," in *IEEE/ACM IWQoS*, Hang Zhou, China, pp. 1–10, Jun. 2020.

[16] X. Liu, Z. Chi, W. Wang, Y. Yao, P. Hao and T. Zhu, "High-granularity modulation for OFDM backscatter," *IEEE/ACM Trans. Networking*, vol. 32, no. 1, pp. 338–351, Jul. 2023.

[17] R. B. Nti, D. K. P. Asiedu and J.-H. Yun, "Nonsequential link adaptation using repetition codes for Wi-Fi backscatter communication," *IEEE Trans. Veh. Technol.*, early access, pp. 1-6, Jan. 2024.

[18] N. Van Huynh, D. T. Hoang, X. Lu, D. Niyato, P. Wang, and D. I. Kim, "Ambient backscatter communications: A contemporary survey," *IEEE Commun. Surveys Tuts.*, vol. 20, no. 4, pp. 2889–2922, 4th Quart., 2018.

[19] C. Xu, L. Yang and P. Zhang, "Practical backscatter communication systems for battery-free Internet of Things: A tutorial and survey of recent research," *IEEE Signal Process. Mag.*, vol. 35, no. 5, pp. 16-27, Sep. 2018.

[20] W. Wu, X. Wang, A. Hawbani, L. Yuan, and W. Gong, "A survey on ambient backscatter communications: Principles, systems, applications, and challenges," *Comput. Netw.*, vol. 216, Oct. 2022.

[21] T. Jiang, Y. Zhang, W. Ma, M. Peng, Y. Peng, M. Feng and G. Liu, "Backscatter communication meets practical battery-free Internet of Things: A survey and outlook," *IEEE Commun. Surv. Tuts.*, vol. 25, no. 3, pp. 2021–2051, 3rd-quarter, 2023.

[22] J. Qian, F. Gao, G. Wang, S. Jin, and H. Zhu, "Noncoherent detections for ambient backscatter system," *IEEE Trans. Wireless Commun.*, vol. 16, no. 3, pp. 1412–1422, Mar. 2017.

[23] J. Qian, F. Gao, G. Wang, S. Jin, and H. Zhu, "Semi-coherent detection and performance analysis for ambient backscatter system," *IEEE Trans. Commun.*, vol. 65, no. 12, pp. 5266–5279, Dec. 2017.

[24] Q. Tao, C. Zhong, H. Lin, and Z. Zhang, "Symbol detection of ambient backscatter systems with Manchester coding," *IEEE Trans. Wireless Commun.*, vol. 17, no. 6, pp. 4028–4038, Jun. 2018.

[25] J. K. Devineni and H. S. Dhillon, "Non-coherent detection and bit error rate for an ambient backscatter link in time-selective fading," *IEEE Trans. Commun.*, vol. 69, no. 1, pp. 602-618, Jan. 2021.

[26] S. Guruacharya, X. Lu and E. Hossain, "Optimal non-coherent detector for ambient backscatter communication system," *IEEE Trans. Veh. Technol.*, vol. 69, no. 12, pp. 16197-16201, Dec. 2020.

[27] Q. Tao, C. Zhong, X. Chen, H. Lin and Z. Zhang, "Maximum-eigenvalue detector for multiple antenna ambient backscatter communication systems," *IEEE Trans. Veh. Technol.*, vol. 68, no. 12, pp. 12411-12415, Dec. 2019.

[28] Q. Tao, C. Zhong, X. Chen, H. Lin and Z. Zhang, "Optimal detection for ambient backscatter communication systems with multiantenna reader under complex Gaussian illuminator," *IEEE Internet Things J.*, vol. 7, no. 12, pp. 11371-11383, Dec. 2020.

[29] T. Kim and W. Lee, "Exploiting residual channel for implicit Wi-Fi backscatter networks," in Proc. *IEEE INFOCOM*, Honolulu, HI, USA, pp. 1-9, April 2018.

[30] G. Wang, F. Gao, R. Fan and C. Tellambura, "Ambient backscatter communication systems: detection and performance analysis," *IEEE Trans. Commun.*, vol. 64, no. 11, pp. 4836-4846, Nov. 2016.

[31] K. Lu, G. Wang, F. Qu and Z. Zhong, "Signal detection and BER analysis for RF-powered devices utilizing ambient backscatter," in *Proc. IEEE Int. Conf. Wireless Commun. Signal Process. (WCSP)*, pp. 1-5, Nanjing, China, Oct. 2015.

[32] Y. Chen and W. Feng, "Novel signal detectors for ambient backscatter communications in Internet of Things applications", *IEEE Internet Things J.*, vol. 11, no. 3, pp. 5388-5400, Aug. 2024.

[33] A. H. Raghavendra, A. K. Kowshik, S. Gurugopinath, S. Muhaidat and C. Tellambura, "Generalized space shift keying for ambient backscatter communication," *IEEE Trans. Commun.*, vol. 70, no. 8, pp. 5018-5029, Aug. 2022.

[34] Z. Niu, W. Ma, W. Wang, and T. Jiang, "Spatial modulation-based ambient backscatter: Bring energy self-sustainability to massive Internet of everything in 6G," *China Commun.*, vol. 17, no. 12, pp. 52-65, Dec. 2020.

[35] Q. Tao, C. Zhong, K. Huang, X. Chen and Z. Zhang, "Ambient backscatter communication systems with MFSK modulation," *IEEE Trans. Wireless Commun.*, vol. 18, no. 5, pp. 2553-2564, May 2019.

[36] J. Qian, A. N. Parks, J. R. Smith, F. Gao and S. Jin, "IoT communications with M-PSK modulated ambient backscatter: Algorithm analysis and implementation", *IEEE Internet Things J.*, vol. 6, no. 1, pp. 844-855, Feb. 2019.

[37] T. Hara, R. Takahashi, and K. Ishibashi, "Ambient OFDM pilot-aided backscatter communications: Concept and design," *IEEE Access*, vol. 9, pp. 89210-89221, 2021.

[38] M. A. ElMossallamy, M. Pan, R. Jäntti, K. G. Seddik, G. Y. Li, and Z. Han, "Noncoherent backscatter communications over ambient OFDM signals," *IEEE Trans. Commun.*, vol. 67, no. 5, pp. 3597-3611, May 2019.

[39] D. Darsena, "Noncoherent detection for ambient backscatter communications over OFDM signals," *IEEE Access*, vol. 7, pp. 159415-159425, 2019.

[40] P. Zhang, M. Rostami, P. Hu, and D. Ganesan, "Enabling practical backscatter communication for on-body sensors" in *Proc. ACM SIGCOMM*, Florianopolis, Brazil, Aug. 2016, pp. 370–383.

[41] A. Wang, V. Iyer, V. Talla, J. R. Smith, and S. Gollakota, "FM backscatter: Enabling connected cities and smart fabrics," in *Proc. USENIX NSDI*, Boston, MA, USA, Mar. 2017, pp. 243–258.

[42] V. Iyer, V. Talla, B. Kellogg, S. Gollakota, and J. Smith, "Inter-technology backscatter: Towards Internet connectivity for implanted devices," in *Proc. ACM SIGCOMM Conf.*, Florianópolis, Brazil, Aug. 2016, pp. 356–369.

[43] D. Li, "Capacity of backscatter communication with frequency shift in Rician fading channels," *IEEE Wireless Commun. Lett.*, vol. 8, no. 6, pp. 1639–1643, Dec. 2019.

[44] J. Morales and A. F. Riveros, "The generalization of the binomial theorem," *J. Math. Phys.*, vol. 30, no. 2, pp. 393–397, Sep. 1989.

[45] F. W. Olver, D. W. Lozier, R. F. Boisvert, and C. W. Clark, *NIST handbook of mathematical functions*. New York, NY, USA: Cambridge Univ. Press, 2010.

[46] J. Proakis and M. Salehi, Digital communication, 5th ed. New York, NY, USA: McGraw-Hill, 2008.

Jixiang Chen received the B.S. degree from Fuzhou University, Fuzhou, China, in 2019, and is pursuing a Ph.D. degree with the South China University of Technology, Guangzhou, China. He is currently a visiting student at Curtin University, Perth, Australia. His research interests include backscatter communications, performance analysis, modulation, and detection.

Quansheng Guan (S'09-M'11-SM'17) received the Ph.D. degree from South China University of Technology (SCUT) in 2011. From 2009 to 2010, he was a visiting Ph.D. student with the University of British Columbia, Canada. From 2012 to 2013, he was a Postdoc Researcher at the Chinese University of Hong Kong. He was a visiting scholar at Singapore University of Technology and Design in 2013, and a visiting professor in Polytech Nantes, France, in 2016. He is currently a full Professor with the School of Electronic and Information Engineering, SCUT.

Dr. Guan is the co-recipients of Best Paper Awards from IEEE ICCC 2014, IEEE ICNC 2016 and ACPEE 2023, Best Demo Award from ACM WUWNET 2018. He is associate editors for IEEE Access, International Journal of Distributed Sensor Networks, and was a guest editor for Mobile Information System. His main research interests are in the areas of wireless networks, underwater acoustic networks, cloud/fog computing, as well as integrated sensing and communications.

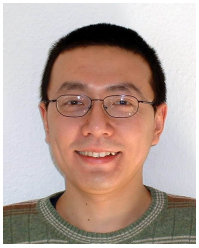

Yue Rong (Senior Member, IEEE) received the Ph.D. degree (summa cum laude) in electrical engineering from Darmstadt University of Technology, Darmstadt, Germany, in 2005.

He was a Postdoctoral Researcher with the Department of Electrical Engineering, University of California at Riverside, Riverside, CA, USA, from February 2006 to November 2007. Since December 2007, he has been with Curtin University, Bentley, WA, Australia, where he is currently a Professor. His research interests include signal processing for communications, underwater acoustic communications, underwater optical wireless communications, machine learning, speech recognition, and biomedical engineering. He has published over 200 journal and conference papers in these areas.

Prof. Rong was a Senior Area Editor of the IEEE TRANSACTIONS ON SIGNAL PROCESSING from 2020 to 2024. He was an Editor of the IEEE WIRELESS COMMUNICATIONS LETTERS from 2012 to 2014 and a Guest Editor of the IEEE JOURNAL ON SELECTED AREAS IN COMMUNICATIONS Special Issue on Theories and Methods for Advanced Wireless Relays. He was an Associate Editor of the IEEE TRANSACTIONS ON SIGNAL PROCESSING from 2014 to 2018.

Dong Li (Senior Member, IEEE) received the Ph.D. degree in Electronics and Communication Engineering from Sun Yat-Sen University, Guangzhou, China, in 2010. Since 2010, he has been with the School of Computer Science and Engineering (formally, Faculty of Information Technology), Macau University of Science and Technology (MUST), Macau, China, where he is currently a Full Professor. He held a visiting position with the Institute for Infocomm Research, Singapore, in 2012. His current research interests focus on 6G Wireless Communications, Battery-Free Internet of Things (IoT) and Wireless AI. He was a recipient of the MUST Best Research Output Award in 2022, and the MUST Bank of China (BoC) Excellent Research Award in 2011, 2016, 2019 and 2021. He was a co-recipient of the Best Paper Awards of IEEE ICCT 2023, IEEE HealthCom 2023, MICCIS 2024 and CCPQT 2024, and the Distinguished Paper Award of IEEE GreenCom 2023. He has been listed among World's Top 2% Scientists recognized by Stanford University since 2020. He is currently an editor for the IEEE MMTC Review, an Executive Board Member of the IEEE Macau Section, and a Member of the Association for Promotion of Science & Technology of Macau.

Weiqi Chen is currently a Lecturer in the School of Internet finance and information engineering, Guangdong University of Finance, Guangdong, China. She received the B.E. degree in Communication Engineering from Sun Yat-sen University, Guangdong, China, in 2008, the M.S. degree from South China University of Technology in 2011, and the Ph.D. degree in School of Electronic and Information Engineering at South China University of Technology, Guangdong in 2019. Her main interests include wireless multi-hop networks and underwater acoustic sensor networks.

Hua Yu (M'06) School of Electronic and Information Engineering, South China University of Technology, Guangzhou, China Key Laboratory of Marine Environmental Survey Technology and Application, Ministry of Natural Resources, Guangzhou, China Hua Yu (Member, IEEE) received the B.S. degree in mathematics from Southwest University, Chongqing, China, in 1995, and the Ph.D. degree in communication and information system from South China University of Technology, Guangzhou, China, in 2004. From 2012 to 2013, he was a Visiting Scholar with the School of Marine Science and Policy, University of Delaware, Newark, DE, USA. He is currently a Professor with the School of Electronic and Information Engineering, South China University of Technology; and an Adjunct Researcher with the Key Laboratory of Marine Environmental Survey Technology and Application, Ministry of Natural Resources, Guangzhou. He is also the Director of the Department of Underwater Communications, National Engineering Technology Research Center for Mobile Ultrasonic Detection. His main research interests include the areas of wireless communications, underwater acoustic communications, and networks. Dr. Yu was a co-recipient of the Best Paper Award from IEEE ICNC 2016 and the Best Demo Award from ACM WUWNET 2018.